Variable Galaxies in the Hubble Deep Field

Vicki L. Sarajedini

Wesleyan University, Middletown, CT 06459

Ronald L. Gilliland

Space Telescope Science Institute, 3700 San Martin Drive, Baltimore, MD 21218

M. M. Phillips

Carnegie Institution of Washington, Las Campanas Observatory, Casilla 601, La Serena,

Chile

accepted _

Received _____;

ABSTRACT

We present results from a study to detect variable galaxies in the Hubble Deep Field North. The goal of this project is to investigate the number density of AGN at $z\simeq1$ through the detection of variable galaxy nuclei. The advantage of HST is the ability to do accurate photometry within smaller apertures, thus allowing us to probe much lower AGN/host galaxy luminosity ratios than can be done from the ground.

The primary data sets analyzed for galactic variability follow from the original HDF-N observations (Williams *et al.* 1996) in December 1995 and a second epoch obtained two years later (Gilliland, Nugent & Phillips 1999). The second epoch data consists of 36 exposures in F814W with a total integration time of 63000 seconds (compared to 58 exposures and a total of 123600 seconds in the original HDF-N).

We have detected nuclear variability at or above the 3σ level in 8 of 633 HDF galaxies at I₈₁₄ \leq 27. Only 2 detections would be expected by chance in a normal distribution. At least one of these 8 has been spectroscopically confirmed as a Seyfert 1 galaxy. Based on the AGN structure function for variability, the estimated luminosity of the varying component in each galaxy lies in the range $-19.5 \leq M_B \leq -15.0$. We construct an upper limit to the luminosity function for the variable nuclei and compare this to the local Seyfert LF and the LF for QSOs at z \simeq 1. Assuming we have detected all Seyfert-like nuclei in the HDF-N, we find no evidence for an increase in the number density of AGN at M_B \simeq -19 (H_o=75 km/s/Mpc, q_o=0.5). From this study, we estimate that \sim 1–3% of field galaxies with I \leq 27 may contain a nuclear AGN.

Subject headings: galaxies: active

1. Introduction

Variability is a well known property of active galaxies. A high incidence of variability has been found among QSO samples (Bonoli *et al.* 1979; Kron & Chiu 1981; Hawkins 1986). Koo, Kron & Cudworth (1986) showed that $\sim 80\%$ of their spectroscopic and color selected quasars in Selected Area 57 (SA57) were variable over the time period of 11 years. In addition to quasars, lower luminosity AGNs such as Seyfert 1s and even Seyfert 2s and LINERs have been shown to exhibit both line and continuum variability (see Aretxaga, 1997 and references therein). Bershady *et al.* (1998) detected 14 extended variable objects in SA57 with Seyfert-like spectral characteristics. The variability amplitude was generally higher for AGN of lower luminosity making this technique well suited for the selection of intrinsically faint QSOs and Seyfert galaxies.

A prominent gap in our current understanding of the AGN phenomenon is the connection between high luminosity QSOs and AGN of lower luminosity. In particular, knowledge of the shape and slope of the low luminosity end of the AGN luminosity function (LF) over a range of redshifts is critical in differentiating AGN evolution models such as pure luminosity, pure density, and luminosity dependent density evolution. Locally, Huchra & Burg (1992) have constructed the LF for spectroscopically selected Seyfert galaxies, but only brighter than $M_B \simeq -18.5$, while Ho *et al.* (1997) have detected fainter nuclei in local galaxies but lack the photometric information to construct the LF. At higher redshifts, however, spectroscopically selected samples as well as most other AGN selection techniques are quickly limited to active nuclei which dominate the host galaxy light and are thus likely to be intrinsically brighter (e.g. Hartwick & Schade 1990). X-ray selection has produced samples of higher redshift, lower luminosity AGN, but without precise optical-to-X-ray flux ratios, these cannot be easily compared with the multitude of optical data for high luminosity QSOs. Through the optical detection of faint, variable nuclei within brighter

1 INTRODUCTION

host galaxies, low-luminosity AGN (LLAGN) can be selected for the purpose of studying the relationship between these objects and higher luminosity QSOs at all redshifts.

In this study, we use HST images of the Hubble Deep Field North separated by 2 years to search for variable objects with emphasis on investigating LLAGN at redshifts of $z\simeq 1$. The advantage of HST is the ability to do accurate photometry within smaller apertures than can be done from the ground, allowing us to probe much lower AGN/host galaxy luminosity ratios.

The primary data sets analyzed for galactic variability follow from the original HDF-N observations (see Williams *et al.* 1996) in December 1995 and a second epoch obtained two years later (Gilliland, Nugent & Phillips 1999, hereafter: GNP). We will only discuss data from the F300W and F814W filters for which extensive observations are available in both epochs (F606W will be brought in as a special case). The second epoch data consists of 36 exposures in F814W with a total integration time of 63000 seconds (compared to 58 exposures and a total of 123600 seconds in the original HDF-N). Also available from the second epoch are 18 exposures in F300W with a total integration time of 27300 seconds (compared to 95 exposures and a total of 178800 seconds in the original). Observations in both epochs were taken using the same orientation (to within a 9' roll difference) and pointing (to $\sim 1''$) on the sky, and each was similarly dithered. Sky background levels were also very similar for the two epochs separated by 731.9 days, or 2.00 years. Critical sampling for the inherently under-sampled WF images is provided by the substantial sub-pixel dithering. The repeated exposures and use of multi-pixel dither offsets in each epoch allow for excellent rejection of both hot pixels and cosmic rays.

We describe the observations and details concerning the galaxy photometry in §2. A description of each variable galaxy AGN candidate detected in the HDF-N is contained in §3. We then compute the luminosity function of variable nuclei in the HDF-N in §4 and

compare it to the local number densities of AGN. In §5 we present a summary of this work and our conclusions.

2. Photometry

2.1. Creation of Over-sampled, Summed Images

A thorough discussion of the data reductions is given in GNP. For each epoch and each bandpass all available frames are combined to produce a single clean image. Hot pixels and cosmic rays are identified and excluded from contributing to the combined image. The individual exposures are taken with different exposure times and varying levels of background light. The combined image production utilizes weights based on readout noise, Poisson statistics on the background and source counts to provide a minimal noise in the final combined, over-sampled image. The adopted algorithm for creation of an over-sampled image uses frame-by-frame registration offsets accurate to ~ 0.02 pixels for F814W and ~ 0.1 for F300W and an accurate model for geometric distortion to maintain optimal resolution. Scattered light patterns affecting a small subset of the images are removed before combining.

To facilitate easy qualitative and quantitative searches for change between the two epochs, the second epoch images are constructed to align with an external galaxy defined reference grid from the first epoch. The resulting alignments are good to maximum errors of ~ 0.05 pixels, or 0''.005. The image for each epoch is scaled to provide the number of e^- per pixel detected in a 6000 second exposure. The same grid of bright external galaxies used to provide registration is used to establish a common intensity normalization (corrections at level of ~1%) for the second epoch relative to the first. With normalized and well registered images for the two epochs a simple difference image provides a sensitive means of detecting

objects that vary in position (some nearby stars) or intensity (AGNs and Supernovae, see GNP for the latter). As an example of the exquisite sensitivity provided by the data, GNP show that 90% of the SNe at $m_{AB(8000)} = 26.4$ in either epoch associated with $z \sim 1.2$ galaxies could be securely detected, with the completeness falling to 50% at $m_{AB} = 27.8$. For the purpose of detecting change with time the extreme stability provided by HST is an important factor in being able to probe to unique magnitude depths with these observations.

2.2. Sensitivity to Photometric Changes for Galaxies

In principle establishing the photometric change for any galaxy is as simple as defining an appropriate aperture and comparing counts in the difference image compared to the counts in the same aperture for the direct image. In the next subsection we will see that the important additional subtlety of changes over time for Charge Transfer Efficiency (CTE) must be dealt with. In the remainder of this subsection we deal with simpler issues of galaxy selection, aperture definition and quantification of expected errors.

We adopt the compilation of 1067 galaxies from Fernández-Soto, Lanzetta and Yahil (1999, hereafter: FLY) for the HDF-N. This is an I-band (F814W) magnitude limited survey comprised of two sets of galaxies from two defined zones in the HDF-N based on the different apparent magnitude depths achievable over the WFPC2 CCDs. The first zone covers the majority of the 3 Wide Field CCDs (3.92 arcmin²) and contains 946 galaxies complete to $m_{AB(8140)}=28.0$. The second zone covers the Planetary Camera CCD and the outer edges of the Wide Field CCDs (1.39 arcmin²) and contains 121 galaxies complete to $m_{AB(8140)}=26.0$.

Each of these galaxies has a photometric redshift based on 7 color (UBVIJHK)

photometry-redshift relations, and where available a spectroscopic redshift from the literature. The photometric redshifts show an rms dispersion of $\sigma = 0.09$ in comparison with a sample of ~100 spectroscopic redshifts at z < 2, with no cases discordant at > 3σ . We have derived a coordinate transform between the x, y positions as tabulated by FLY and our factor of 4 over-sampled images; this is accurate to ≤ 10 of our pixels (or 0".25). We then adopt the pixel with maximum counts within ± 20 over-sampled pixels as the nominal center of each galaxy.

Williams *et al.* (1996) tabulate a first moment radius for each galaxy. For an $r^{1/4}$ light distribution the half-light radius is one-half the first moment radius, and we have simply adopted one-half the first moment radius for each galaxy as a nominal scale for an aperture on each galaxy. Figure 1 shows the distribution of galaxy half-light radii as a function of apparent magnitude for the FLY sample.

With a minimum aperture size of 0.05'', the aperture photometry for some of the galaxies essentially returns the central pixel value in each epoch. There is no reason to declare this a suspect value. First, the typical variation in the intra-pixel QE response is 1 to 2%, depending upon where a point source is centered within the pixel. This is reduced in amplitude by the square root of the number of dithers to different sub-pixel coordinates resulting in an error of $\leq 0.5\%$. At these magnitudes, the intrinsic random errors are already ten times this value. Second, time dependent gain variations over the entire chip are calibrated out in establishing differential photometry with a mean of zero across epochs. Furthermore, time dependent gain variations for individual pixels, however unlikely, would be eliminated when producing our combined images.

At $m_{AB(8000)} = 26.0$ an integrated object count level of ~ 310 e^- is accumulated in 1750 seconds (average exposure time of second epoch data). At a half-light radius of 0".2 half of this light would be spread over 4π pixels (0".1, WF), or ~ 12.3 e^- per pixel. The sky

level per exposure is about 78 e^- per pixel on average. If we make the reasonable estimate that the local sky can be defined to ~ 1 e^- per pixel, then with an aperture of 0"2 at m =26 the uncertainty from possible zero point errors on the sky is 8%. The intrinsic Poisson, sky and readout noise limited S/N (within the half-light radius) in this example would be ~ 24 in the shallower 2nd epoch and ~ 34 in the original HDF. At an uncertainty of 1 e^- in the zero point of the difference image, photometric errors from this term alone are 60% larger than the intrinsic S/N limit (5%, 1 σ) of the difference image. In order to not have uncertainties in the sky zero point dominate the errors we have adopted aperture radii which are the minimum of tabulated values and the quadratic relation plotted in Figure 1. Adoption of this smaller radius, which is set at a point between the lower envelope and the mid-point of measured radii, effectively removes uncertainties in the sky zero point from major importance in an error budget.

Having defined an aperture choice the fractional change in photometric intensity for any source is just the summed counts over this aperture in the '97 - '95 difference image divided by the summed counts in a grand average image. In order to search for variable galaxies we now need to establish the expected noise level of this measure for non-variable objects. GNP developed two sets of "null experiments" to help quantify the level beyond which random noise could be misinterpreted as Supernovae. The control images that result from these null experiments are also ideal for establishing the expected galaxy-photometry measurement noise as a function of magnitude.

One null experiment consists of dividing the full set of individual exposures into two sets, one composed simply of the odd numbered frames and the other the even numbered ones. Each set is now an "epoch", but with no real time difference. The difference image from these even and odd epoch combined frames effectively carries through the effects of object and sky Poisson noise, readout noise, and any limitations imposed by minor errors

in the sky zero points used. However, no intrinsic variations (on timescales greater than exposure times of individual frames) can exist and the apparent variations in photometry between the sets can be used to define the noise-magnitude relation.

As a second null experiment, GNP had also defined simulated images for each epoch starting with the same over-sampled and optimally combined representation of the source distribution and non-variable background light (noiseless relative to levels in individual exposures). These combined images are represented as bi-cubic surface fits to the light distribution over individual WFPC2 pixels as a function of sub-pixel x and y offsets. As such these can be evaluated at the offset position of any individual exposure and an amount of noise appropriate to readout, dark current, sky background and source Poisson statistics added to simulate each individual exposure. The simulated frames for each epoch were then recombined to produce an over-sampled image for each epoch. Again, this should capture most sources of noise, but no real variations can exist.

Figure 2 shows the adopted 1σ galaxy photometry error as a function of magnitude. This represents a sum over results for the two independent null experiments for which the differences between the two were small. The apertures used here and throughout the paper are as shown in Figure 1, namely for each galaxy the minimum value of the tabulated half-light radius and the quadratic function of magnitude. The magnitudes adopted from here on (referred to as $m_{AB,int}$ later) apply to the intensity level internal to the adopted half-light radii. An appropriate zero point offset is adopted to bring the mean of these generally smaller aperture magnitudes into registration with the FLY isophotal magnitudes. The data points represent the rms photometry differences for all galaxies within ± 0.45 magnitude intervals at m = 22 with this interval decreasing to ± 0.25 mag at m = 27 from the two sets of null experiments. Note that the simple first principles argument developed earlier gave an error of 5% at m = 26 in excellent agreement with this calibration. The

distribution of errors in any magnitude bin for the null experiments is well centered on zero and has a Gaussian distribution. A lower limit to the assumed photometric error of 0.012 magnitudes was adopted based on general experience with absolute limits to WFPC2 photometric accuracy. Our conclusions are not sensitive to reasonable bounds on this limiting precision.

A direct solution for photometric changes of real galaxies, normalized to the typical expected error as a function of magnitude can now be easily evaluated. Figure 3 shows the distribution of photometric changes both as direct delta intensities across the two epochs and after normalizing these to the expected errors as a function of magnitude. The results showed a very non-Gaussian distribution with 33 galaxies out of the brightest 633 (selected on the basis of $m_{AB(8140)} < 27.5$ for the standard apertures as shown in Figure 1) showing $> 3\sigma$ variation compared to statistically expecting 2 of 633 by chance for a normal distribution. Either the rate of variable galaxies in the HDF far exceeds the canonical fraction of $\sim 2\%$ for AGNs, or we have unaccounted for noise or systematic errors. Inspection of the photometric differences across epochs showed clear correlations with magnitude and with y-position on the CCDs. Such behavior is suggestive of a CTE systematic error term. In our case, since we are comparing data acquired with similar exposure times and nearly identical pointings, such an effect would follow only from a change of CTE with time.

2.3. The Role of Charge Transfer Efficiency Changes

We have solved empirically for corrections to the photometry with a simple linear model of time differential CTE having linear terms in magnitude and source position on each CCD. An ideal solution will eliminate any systematics in photometry differences between epochs. Experimentation showed that any effect in x must be significantly smaller than for y, and not finding any consistency across CCDs the x-dependence for time-differential CTE was taken to be zero. Generally consistent values for a CTE term with linear dependence on y were found across the CCDs, and with restricting the solutions to either bright ($m = 24.5 \pm 1.0$) or faint ($m = 26.5 \pm 0.5$) galaxy sets. The full range scatter for this term is \pm 20% evaluated separately for the 3 WF CCDs and the m = 24.5 set of galaxies; we have adopted the mean values independent of CCD. The linear correlation coefficients of relative intensity differences against y-position ranged from 0.23 to 0.32 (correlations against xspanned -0.09 to 0.02). The adopted CTE (time difference '97 - '95 epochs) is:

$$C = -0.029 + 0.006 * (24.5 - m_{AB}) - 1.0 \times 10^{-5} * (y - 1600).$$
(1)

The sign of each term is consistent with a slightly increased CTE loss over the two years between the HDF epochs. The magnitude of the slope in y produces a 3.2% effect bottom to top. Since for galaxies at $m_{AB} \sim 24.5$ the assumed intrinsic noise is $\sim 2.4\%$, such an overall slope is a significant bias. Figure 4 shows the solution for a y-dependent correction factor for WF4 for which the linear correlation coefficient is -0.29.

Our solution for a CTE effect is in a unique range of parameter space compared to previous calibrations. In particular our correction primarily applies to objects that have a comparable, or smaller per pixel count level than local sky in individual exposures. Published calibrations for CTE (Whitmore 1998, Stetson 1998) have generally relied on well exposed stars (at least by the HDF standards) for which a typical star image would peak at > 10³ photoelectrons per pixel with an ambient diffuse sky brightness of ~ 10 e^- per pixel. Even for "bright" galaxies in the HDF with $m_{AB} = 24.5$ and a median half-light radius of 0?15 the average count level for pixels within this radius is 87 e^- compared to typical sky of 78 e^- . Whitmore (1998) found an increased loss attributed to a change of CTE for faint stars with ~ 40 e^- per pixel (average within a 0?2 radius aperture) equal to 9.5 ± 3% (center of CCD) over a 3 year baseline. The HDF galaxies have smaller to comparable

count levels, but are relative to a higher sky level (which will suppress the loss) compared to the calibration described by Whitmore (1998). Stetson (1998) found a much smaller time dependence of ~ 1% over 3.5 years analyzing a more extensive set of data.

We note that a small relative component (10% of total) of our derived time dependent CTE change can simply be attributed (using the Stetson 1998 equations) to our use of shorter exposure times on average for the second epoch (1750 s) compared to the original F814W HDF exposures (2130 s). Our derivation of the time-differential CTE effect is well defined empirically for the two epochs of HDF galaxy photometry, and given the suppression from a larger ambient sky background is generally consistent with the changes found by Whitmore (1998). The Whitmore analyses are done differentially comparing WFPC2 photometry acquired after large scale changes of stellar position on the CCDs; the Stetson analyses for CTE directly adopt a comparison with ground based, crowed-field photometry. Published time dependent CTE results at significant amplitude only apply to the very faintest stars, for these, ground based systematic errors may not be negligible and may explain the different level of effect found in the studies. In any case the several hundred galaxies available in the HDF, ~ 99% of which are non-variable, have been used here to provide an empirical correction for time-dependent CTE changes that for these two epochs of F814W data is reliable and accurate for our purposes.

2.4. Photometric Changes of HDF Galaxies

With a solution for time-differential CTE included, any remaining systematic errors in galaxy photometry across epochs will be small compared to random errors per galaxy. Figure 5 shows the full set of corrected galaxy intensity differences between the two epochs. Details for all galaxies with changes relative to the expected error (Figure 2 relation) larger than 3σ are given in Table 1, with column definitions of: (1) Galaxy number from Williams et al. 1996. (2) Isophotal F814W magnitude in AB system from FLY. (3) m_{AB} internal to the adopted half-light radius. (4) Redshift from FLY based on spectroscopic determination if available (s) or photometric (p). (5) Fractional change in intensity across epochs within $r_{1/2}$; positive implies brighter in 2nd epoch. (6) Significance of change obtained by ratioing to the expected error as a function of magnitude (Figure 2). (7) Half-light radius as minimum of one-half the Williams et al. (1996) first-moment radius and the quadratic function plotted in Figure 1. (8) Separation between centroid of excess light and the galactic nucleus. (9) Absolute value of the magnitude difference between the two epochs. Results are tabulated only for the 633 galaxies which have $m_{AB,int}$ (column 3 of Table 1) brighter than 27.5.

Figure 6 shows the cumulative distribution of the variability significance (the ratio of the change in magnitude to the expected error at that magnitude) for all of the galaxies considered in the study. This value is given in column 6 of Table 1 for the 9 variable galaxies. We show the cumulative distribution (solid line), the fit to these points at δ/σ < 2.7 (dashed line), and the positions of the 9 variable galaxies along the x-axis. A clear excess of galaxies can be seen beyond $\delta/\sigma = 2.7$. The area under the dashed line beyond $\delta/\sigma = 2.7$ translates to approximately 2 galaxies, the number that would be expected in a normal distribution to have variability significance greater than 3σ . From this figure, it is clear that there is an excess of objects having a variability significance of greater than 3 (we have set the selection threshold at the traditional 3σ level, slightly higher than the break at 2.7).

Of the nine variable galaxies listed in Table 1, 4-403.0 has been thoroughly discussed in GNP. The brightening in 4-403.0 has been attributed to a Supernova (SN1997ff) detected in the second epoch data. The residual light associated with 4-403.0 from subtraction of the first epoch from the second is well represented as a point source 0.16 off the galaxy nucleus

with $m_{AB} = 27.4$. This brightness is consistent with a Type Ia SN at the galaxy redshift of z = 1.32 detected ~ 40 days (observer's frame) after maximum. This off-center brightening was judged much more consistent with a SNe interpretation than as AGN variability. A second SN (SN1997fg) associated with galaxy 3-221.0 was also reported in GNP; it was not picked up in this galaxy variability search since the SN was well outside the half-light radius summed over for 3-221.0.

The Supernova search used a different approach of detecting point sources present in a difference image of the two epochs independent of knowledge of galaxy positions (except for scaling errors up appropriately to account for increased Poisson noise based on count levels). The variable sources 2-251.0 and 3-404.2 were also briefly discussed in GNP. In these cases the brightening comes from an apparent point source coincident with the galactic nuclei within small measurement errors. For 3-404.2 with a half-light radius of 0''.15 the formal offset of the first epoch excess light was 0''.048 from the galaxy center (consistent with zero) and the amount of galaxy light within a radius of 0''.05 is $\sim 4\%$ of the total making interpretation as an AGN more likely than as a SN. For 2-251.0 there is abundant supporting evidence in the literature (see §3) that this is an AGN.

The next to last column of Table 1 gives the apparent radial offset (δr) of the excess light in one epoch from the galaxy nucleus. The error on this measurement is typically about 0''.05. In all cases, except for 4-403.0 for which we believe the brightening in the second epoch was caused by SN1997ff, the estimated δr is well under the estimated half-light radius. Coincidence with the nucleus alone cannot establish whether a specific event should be attributed to AGN activity or a SN, but statistically the SNe would be expected outside the $r_{1/2}$ radius as often as inside. The strong bias for the excess light centroids in Table 1 to align with the galactic nucleus to a level well under the half-light radius supports interpretation of these events as AGN.

2.5. Additional Photometric Change Measures for 2-251.0

From inspection of Table 1 it is clear that 2-251.0 is in a class by itself. The absolute magnitude of the excess light across the epochs at $m_{AB} \sim 23.5$ is a factor of 20 brighter than the next brightest at ~ 26.7. Furthermore, even with the comparison of 63000 seconds in F814W with the original longer HDF, 27th magnitude is where errors are becoming large. From inspection of the two epochs of F300W data (2nd epoch only 15% as long as the original) it is obvious that: (1) 2-251.0 is clearly visible and exhibits change. (2) None of the other AGN/SNe candidates are even close to detection in F300W.

We searched the Hubble Archive for any other pairings of HDF exposures giving temporal information on the brightness of 2-251.0. The pre-HDF test of guide stars six months before the original HDF included three F606W exposures with a total exposure time of 2200 seconds with 2-251.0 present on WF3 at x, y = 252,410.

Table 2 summarizes the available photometry for 2-251.0. Over six months just prior to the HDF the F606W observations are consistent with no change, or a slight increase of flux. Over two years after the original HDF galaxy 2-251.0 brightened by ~ 8% in F814W (rest wavelength ~ 4100 \pm 250 Å) and by ~ 40% in F300W (rest wavelength ~ 1500 \pm 200 Å).

3. The Variable Galaxies

Figure 7 is a composite of the I-band images of the eight variable galaxies that are candidate AGNs from Table 1. These galaxies meet the criterion for having nuclear variations in excess of 3σ above the background noise. However, we note that two such galaxies would be expected to appear as 3σ variables statistically in a normal distribution as discussed in §2.4. Each pair of images consists of the I-band image of the galaxy on the left and the difference image of the two epochs shown to the right (first epoch subtracted from the second epoch observation). The gray scale has been adjusted so that the variable region is always positive (black). The dash at the bottom right in each frame represents the 1kpc scale for the galaxy. The galaxies appear to cover a range of Hubble types and magnitudes. We briefly discuss each of the galaxies below.

2-251.0 - This red galaxy at z = 0.96 (spectroscopic) is the most variable galaxy in our survey with a magnitude excess of 23.5 mag over the 2 year period. This galaxy also has an interesting morphology. Two-dimensional model fitting finds a prominent bulge component (Marleau & Simard 1998) although spiral-like structure is also seen out to ~0.6" from the nucleus. The spectrum for this object reveals broad MgII (2800Å) emission (Phillips *et al.* 1997; Songaila 1997) which is further evidence that this object contains an AGN. In addition this object is also a radio source having been detected in the VLA survey of the HDF-N (Richards *et al.* 1998; Fomalont *et al.* 1997). The VLA observations also report variability of this source by about 30% over an 18 month period. The radio spectral index is $\alpha = -1.0\pm0.1$ further suggesting the AGN nature of this object. This galaxy was also detected by ISO having S_{7µm}=52µJy (Rowan-Robinson *et al.* 1997). Although they suggest this source is a massive starburst with a SFR of 200 M_☉/yr, the corroborating evidence seems to suggest that the presence of an AGN is the more likely explanation.

4-260.111 - This galaxy has a spectroscopic redshift of 0.96 and appears to be a late-type spiral galaxy with 2-dimensional model fitting indicating little or no bulge component. The variability is off-nucleus by 0.1" although this is well within the half-light radius of the galaxy. This object is also an ISO source with $S_{7\mu m}=51\mu Jy$ (Rowan-Robinson *et al.* 1997).

2-210.0 - This galaxy with a spectroscopic redshift of 0.75 also appears to be a spiral with little or no bulge component. The disk is "blobby" appearing to have several HII-like regions in the spiral arms. The peak in the variability is very close (0.03'') to the nucleus of

this galaxy.

3-266.0 - Two-dimensional model fitting of this galaxy indicates the presence of a large bulge component. The small half-light radius (0.1'') is further evidence that this galaxy is elliptical. A spectrum has just recently been obtained for this object (Cohen et al. 2000) and the redshift is 0.95.

3-404.2 - This galaxy has a spectroscopic redshift of 0.52. It has a moderate bulge component (B/T=0.3 from Marleau & Simard 1998) and is probably an Sa-type spiral galaxy.

2-787.0 - This galaxy has a photometric redshift of 0.92. The model fitting indicates a small bulge fraction (B/T=0.08). This galaxy, in addition to the last two, are the least variable galaxies to meet the selection criterion.

4-327.0 and 4-344.0 - These two galaxies are very faint making their morphologies difficult to classify. Their photometric redshifts place them at 1.9 and 1.4 respectively. These are likely to be dwarf galaxies having absolute magnitudes around $M_I \simeq -17.5$.

Although spectroscopic data exists for 5 of the AGN candidates selected in this study, the spectra themselves or information regarding their spectral properties were only available for object 2-251.0 at the time of publication.

4. Comparison with the Local Number Density of Seyferts

One issue we would like to address with the results of this study is the evolution of the number density of AGN. Of the nine variable galaxies detected, we are confident that one (4-403.0, see Gilliland, Nugent and Phillips 1999) is a supernovae. The majority of the remaining 8 are likely to be AGNs with the caveat that two of these would be expected statistically from the noise distribution tail. By comparing the number density of these variable galaxies at $\langle z \rangle \simeq 1$ to the local number density of Seyfert galaxies, we can place limits on any significant evolution of the population of AGNs over this redshift range.

4.1. The Luminosity Function of the Variable AGN

To compare the number density of variable AGN detected within HDF-N galaxies to that of local Seyferts, we require an estimate of the absolute magnitude of the AGN component in each of the variable galaxies. To make this estimation, we must approximate the expected level of variability for each AGN. Then, based upon the amount of variability observed for each galaxy, we can estimate the fraction of the flux that is due to the AGN. It is difficult, however, to know the precise variability amplitude expected for a given AGN. Many studies have shown that the amplitude of variability depends on the AGN luminosity (Trevese *et al.* 1994, Hook *et al.* 1994). Unfortunately, surveys of low-luminosity AGN variability have not yet been completed and therefore, little exists in the way of statistical results which quantify the amount of variability expected for the active nuclei we are trying to detect in this study. At this point, the best we can do is estimate the amount of variability expected for our nuclei based on the results of larger variability surveys of intrinsically brighter QSOs and attempt to extrapolate to lower luminosities based on the apparent trends in amplitude with magnitude.

We adopt the structure function results from Hook *et al.* (1994) to estimate the expected variability amplitude for our AGN over a given time interval. The structure function was calculated from a sample of ~ 300 optically selected quasars studied over a period of 16 years at seven epochs. From this sample of QSOs, an amplitude variation with respect to absolute magnitude was detected. The structure function is fit with the equation

$$S = \sqrt{[0.155 + 0.023(M_B + 25.7)]t^p}$$
(2)

where M_B is the absolute magnitude of the QSO. When the observed time interval t is known, this equation yields the expected amplitude of variability in magnitudes for a QSO. The value t in equation 2 is two years for an object at z=0 in the HDF images used in this study. However, higher redshift objects have decreasing values of t due to time dilation effects. To determine the true observed time interval for each galaxy, the actual observational time interval of 2 years must be divided by $(1+z_{gal})$ such that a galaxy at z=1 would have t=1 year. The redshifts we use are a combination of spectroscopic redshifts when available and photometric redshifts (FLY).

With equation 2, we estimate the expected amplitude of variability for each AGN and determine the fraction of the galaxy flux due to the AGN component based on the observed variability of the galaxy. In combination with the known redshift, we then know the absolute magnitude of the galaxy and AGN component. The Hook et al. sample included only QSOs with $M_B \leq -23.0$ so to apply these results to our data, we must extrapolate to lower luminosities. Since the structure function equation used to determine the AGN magnitude is also a function of that magnitude, we use an iterative method to arrive at a magnitude estimate. We start by assuming M_B =-23.0, determining the AGN magnitude from the variation amplitude calculated from equation 2, and then inputing this new AGN magnitude into the equation to redetermine the expected level of magnitude variation. We continue this process until we reach the AGN magnitude which satisfies the equation and the observed level of magnitude variation. In all cases, this point was reached within three iterations. The estimated absolute magnitude range for our AGN is $-19.5 \leq M_B \leq -15.0$. The absolute magnitude of the AGN, as estimated from the structure function, has an associated error of $\pm \sim 0.25$ mag which falls well within the bin size used to to construct the luminosity function below.

The luminosity function is computed using the $1/V_a$ technique (Schmidt and Green

1983) where V_a is the accessible volume over which each object can be observed in the survey. For computing the LF, we consider only zone 1 of the HDF which comprises the majority of the 3 Wide Field chips, covering 3.92 arcmin². All of our AGN candidates fall within this region of the CCD.

From the total integrated magnitude of the galaxy, we determine the distance at which each object could be observed within the surveys' apparent magnitude limit. We then determine the distance where the variability amplitude of the AGN within the host galaxy falls below the 3σ variability selection threshold. The accessible volume, V_a , is then determined from the closer of these two distances. Table 3 lists the absolute magnitude for each variable nucleus included in the LF calculation as well as the apparent I magnitude, the maximum redshift over which the object could be observed (z_{max}), and V_a for each object in Mpc³. The LF is the summation of $1/V_a$ for each object divided into two absolute magnitude bins centered on M_B =-15.75 and -18.25 (Figure 8). The luminosity function is tabulated in Table 4.

The determination of the apparent magnitude limit of the survey is an important aspect of the LF calculation. The number counts of the HDF-N galaxies in FLY appear to turn over at ~26.5 to ~27. We also note that FLY indicate that the median redshift of their galaxy catalog steadily increases up to $I_{AB}=26.0$ and then remains fairly constant. To avoid incompleteness due to surface brightness selection effects as well as possible redshift incompleteness we have set the apparent magnitude limit for the calculation of the LF at $I_{AB}=26.0$. In doing this, we must remove the two faintest variable sources, 4-327.0 and 4-344.0, from our LF calculation since their integrated galaxy magnitudes fall below this magnitude cut-off. These objects also have the highest estimated redshifts among our candidates ($z_{phot}>1$) as well as displaying some of the lowest variability significance according to Figure 6.

4.2. Discussion of the Luminosity Function

Figure 8 is the resulting LF for the 6 brightest variable galaxies in the HDF-N. We compare the LF for the variable galactic nuclei in the HDF-N (squares) with the local Seyfert LF (Seyfert 1s and 2s) from Huchra & Burg (1992) (filled circles) and the QSO LF at $\langle z \rangle =1$ from Hartwick & Schade (1990) (asterisks). We have converted our I magnitudes for the variable HDF galaxies into B magnitudes and applied a K-correction based upon the redshift assuming a power-law spectrum for the AGN candidates with $\alpha =-1.0$. With these assumptions, the K-correction is zero and I_{AB} -B_{Johnson}=-0.64. The error bars represent the Poisson errors based on the number of objects in each bin. Due to the small number of objects used in constructing this LF, we have chosen a large bin size (2.5 magnitudes) to reduce the statistical error per bin.

The most remarkable feature of this figure is the smooth transition between the local Seyfert LF and our AGN candidates from the HDF. We note that our AGN LF extends to fainter magnitudes than the local LF even though our data are at higher redshifts ($\langle z \rangle = 0.84$) demonstrating the strength of this detection technique. In the luminosity range where our LF overlaps the local Seyfert LF, there is no evidence for an increase in number density. Within the error bars, the number of AGN at $-18.5 \ge M_B \ge -19.5$ remains the same for the local and higher redshift LFs. This is in stark contrast to the situation at brighter absolute magnitudes ($M_B \le -23.0$) where the number density appears to increase significantly between local and higher redshift surveys.

The shape of our LF, although comprised of only two luminosity bins, does display the trend of increasing number density with fainter absolute magnitude. The bin centered at M_B =-15.75 is higher than that at -18.25 at greater than the 1 σ significance level. Although clearly more AGN are necessary to verify this trend, this initial study points toward the possibility that AGN number counts have not turned over by $M_B\simeq$ -16 but continue to

increase at these faint magnitudes. More data are needed to determine the behavior of the faint end of the AGN LF with greater statistical significance.

5. Summary and Conclusions

With the goal of investigating the number density of AGN at $z\simeq 1$, we have completed a survey of variable galaxies in the Hubble Deep Field North. Through the detection of Seyfert-like galaxies based on their variable properties, we hope to help bridge the gap between luminous QSOs and intrinsically fainter AGNs at higher redshifts. This initial study demonstrates the power of this technique for detecting Seyfert galaxies or low-luminosity AGN at $z\sim 1$.

Out of 633 galaxies with $I_{int} \leq 27.5$, we have found 8 galaxies which appear to be varying at $\geq 3\sigma$ over the two year period. These galaxies, at $\langle z \rangle \sim 1$, cover a range of absolute magnitudes, colors, and hubble types although the majority appear to have some spiral structure. At least one is a confirmed Seyfert 1 galaxy based on spectroscopic and radio observations.

We have estimated the magnitudes for the variable nuclei found in HDF-N galaxies by adopting a structure function for QSO variability. By estimating the expected variability amplitude for each candidate AGN, we can disentangle the AGN flux from that of the underlying galaxy and determine the magnitude of the varying nucleus. We estimate the nuclear magnitudes to lie in the range $-19.5 \leq M_B \leq -15.0$.

The comparison of the luminosity function for our variable nuclei to that for local Seyferts does not indicate any number density evolution for AGN at $M_B \simeq -19$. This variability selection technique, however, may result in an underestimate of the number of AGN due to the fact that every AGN may not display variability over the 2 year timescale

5 SUMMARY AND CONCLUSIONS

we have studied. Although it is difficult to know exactly what fraction of AGN we have detected, we can make an estimate based upon previous QSO variability studies. The study of SA57 (Trevese *et al.* 1994; Bershady *et al.* 1998) finds that virtually all of the known quasars in this field were detected to be variable. They also point out that the fractional variability amplitude, being higher for lower luminosity AGN, suggests an even higher success rate for Seyfert-like galaxy detection, consistent with the results of Hook *et al.* (1994). A recent study by Giveon *et al.* (1999) confirms this anticorrelation between variability amplitude and luminosity. This study of 42 optically selected PG quasars also finds that all were variable over the 7-year study period. Based upon the published amplitude gradients, we would estimate that ~90% would have been detected in our survey over the 2-year period given our typical photometric errors.

Therefore, we estimate that the majority of Seyfert-like galaxies in the HDF-N would be detected in our variability survey. With a conservative estimate that the detection rate is between 50 and 90%, the total number of variable galaxies in the HDF-N at I \leq 27 represents ~1–3% of all galaxies at this magnitude limit. Our result is consistent with the findings of Sarajedini *et al.* (1999) where the fraction of field galaxies containing an AGN is estimated based on the presence of an unresolved nuclear component. In this study, the fraction of galaxies containing a nuclear point-source in HST imaged galaxies to z~0.8 was determined as a function of the nucleus–to–host galaxy luminosity ratio. The variable galaxies in the HDF-N are likely to contain AGN components that comprise at least 15% of the total galaxy light estimated from the observed level of variability in each selected galaxy. Sarajedini *et al.* find that ~3% of their field galaxies contain nuclear components which make up \geq 15% of the galaxy's light, consistent with the results of this study.

As larger variability surveys of field galaxies are conducted with longer temporal baselines, the number of low-luminosity AGNs detected will increase allowing for more statistically complete studies of this population of objects. The results of this study demonstrate the strength and efficiency of this technique to select low-luminosity AGN candidates at moderate redshifts.

We would like to thank David Koo for many helpful suggestions and comments on this paper. We also thank the referee for carefully reading this paper and making several suggestions to help improve it. Support for this work was provided by NASA through grant number AR-7984.02-96A from the Space Telescope Science Institute, which is operated by the Association of Universities for Research in Astronomy, Inc. under NASA contract NAS5-26555. V.L.S. completed part of this work while at the Astronomy and Astrophysics Department at UC Santa Cruz.

R.L.G. acknowledges the hospitality of the Astronomy and Astrophysics Department at UC Santa Cruz where much of this work was done, and the ST ScI for a sabbatical leave, and support via GO-6473.01-95A and AR-7984.01-96A.

5 SUMMARY AND CONCLUSIONS

REFERENCES

- Aretxaga, I. 1997, RevMexAA, 6, 207
- Bershady, M.A., Trevese, D. & Kron, R.G. 1998, ApJ, 496, 103
- Bonoli, F., Braccesi, A., Federici, L., Zitelli, V., & Formiggini, L. 1979, A&AS, 35, 391
- Cohen, J. G., Hogg, D. W., Blandford, R., Cowie, L. L., Hu, E., Songaila, A., Shopbell, P., and Richberg, K. 2000, ApJ, in press.
- Fernández-Soto, A., Lanzetta, K.M., & Yahil, A. 1999, ApJ, 513, 34 (FLY)
- Fomalont, E.B., Kellermann, K.I., Richards, E.A., Windhorst, R.A. & Partridge, R.B. 1997, ApJL, 475, L5
- Gilliland, R.L., Nugent, P.E., & Phillips, M.M. 1999, ApJ, 521, 30 (GNP)
- Giveon, U., Maoz, D., Kaspi, S., Netzer, H. & Smith, P.S. 1999, MNRAS, 306, 637
- Hartwick, F. D. A. & Schade, D. 1990, ARA&A, 28, 437
- Hawkins, M.R.S. 1986, MNRAS, 219, 417
- Ho, L.C., Filippenko, A. & Sargent, W.L.W. 1997, ApJS, 112, 315
- Hook, I. M., McMahon, R. G., Boyle, B. J. & Irwin, M. J. 1994, MNRAS, 268, 305
- Huchra, J. & Burg, R. 1992, ApJ, 393, 90
- Koo, D.C., Kron, R.G. & Cudworth, K.M. 1986, PASP, 98, 285
- Kron, R.G. & Chiu, L.-T. 1981, PASP, 93, 397
- Marleau, F.R. & Simard, L. 1998, ApJ, 507, 585
- Phillips, A.C. et al. 1997, ApJ, 489, 543
- Rowan-Robinson, M. et al. 1997, MNRAS, 289, 490

- Richards, E.A., Kellermann, K.I., Fomalont, E.B., Windhorst, R.A. & Partridge, R.B. 1998, AJ, 116, 1069
- Sarajedini, V.L., Green, R.F., Griffiths, R.E., & Ratnatunga, K.U. 1999, ApJS, 121, 417
- Schmidt, M. & Green, R.F. 1983, ApJ, 269, 352
- Songaila, A. 1997, The Hawaii Active Catalog of the Hubble Deep Field, http://www.ifa.hawaii.edu/~cowie/tts/tts.html
- Stetson, P.B. 1998, PASP, 110, 1448
- Trevese, D. & Kron, R.G. 1990, in Variability of Active Galaxy Nuclei, ed. H.R. Miller & J.P. Witta (Cambridge:Cambridge Univ. Press), 72
- Trevese, D., Kron, R.G., Majewski, S.R., Bershady, M.A. & Koo, D.C. 1994, ApJ, 433, 494
- Whitmore, B. 1998, Technical Instrument Report WFPC2 98-01 (Baltimore: ST ScI)

Williams, R.E. et al. 1996, AJ, 112, 1335

This manuscript was prepared with the AAS ${\rm IAT}_{\rm E}{\rm X}$ macros v4.0.

FIGURE CAPTIONS

Fig. 1.— Half-light radii (half of first moment radii from Williams *et al.* 1996) in "plotted against isophotal F814W AB magnitudes from FLY. The quadratic curve shows the adopted aperture radius for cases in which this is less than the tabulated half-light radius.

Fig. 2.— Plus signs show *rms* of photometric relative intensity differences between galaxies in the null experiments discussed in the text within given magnitude intervals. The curve is a quadratic fit supplemented with a minimum value of 0.012.

Fig. 3.— The upper panel shows the relative intensities of the HDF galaxies as the difference of '97 minus '95 real data epochs relative to the grand average data image intensity. The lower panel shows the intensity differences after a magnitude dependent normalization to the function plotted in Figure 2. These are for intensity comparisons before application of the CTE corrections discussed in §2.3. Note the asymmetric distribution relative to the zero line, and the large number of galaxies apparently variable at > 3σ levels. The solid lines in the lower panel indicate the 0 and 3σ levels.

Fig. 4.— Demonstration of y-dependent CTE term showing the distribution of intensity differences between the two epochs plotted against y - 1600 (in our over-sampled by 4 data). The ~ 3.2% CTE effect bottom to top of the WFPC2 CCDs (time-differential across two years) introduces a strong photometry error if not corrected for.

Fig. 5.— The intensity differences for the HDF galaxies after correction for the timedependent CTE are plotted in the upper panel. The lower panel shows the same following normalization by expected random errors per galaxy. Again, the solid lines in the lower panel indicate the 0 and 3σ levels. The 9 galaxies varying by more than 3σ at I(AB)<27.5 are labeled.

5 SUMMARY AND CONCLUSIONS

Fig. 6.— The cumulative distribution of the variability significance (the ratio of the change in magnitude to the expected error at that magnitude) for all of the HDF-N galaxies to $m_{AB(8140)}=27.5$ (solid line). The fit to the data at $\delta/\sigma < 2.7$ is shown as the dashed line. The positions of the 9 variable galaxies are marked along the x-axis.

Fig. 7.— I_{F814W} band image of the eight variable galaxies (left) and the difference image between the two epochs (right). The white circle on the difference image indicates the peak in variability. The dash at the bottom right corner of each frame represents the length of 1kpc in the rest-frame of each galaxy.

Fig. 8.— The luminosity function for our 6 AGN candidates having integrated galaxy magnitudes brighter than $m_{AB(8140)}=26$ (filled squares). We compare our LF with the local combined Seyfert 1 and 2 LF of Huchra and Burg (1992) (filled circles) and the QSO LF at $\langle z \rangle = 1$ (Hartwick and Schade 1990) (asterisks).

ID (1)	m_{AB} (2)	$m_{AB,int}$ (3)	z (4)	δ_{int} (5)	δ_{int}/σ (6)	$r_{1/2}('')$ (7)	$\frac{\delta r(")}{(8)}$	$m_{AB,excess}$ (9)
2-251.0	21.24	20.76	0.96 s	0.08	6.73	0.23	0.03	23.49
4-260.111 2-210.0	22.55 22.69	23.85 23.75	0.96 s 0.75 s	$\begin{array}{c} 0.06 \\ 0.05 \end{array}$	4.39 3.69	0.21 0.20	$\begin{array}{c} 0.11 \\ 0.03 \end{array}$	26.88 27.03
3-266.0 3-404.2	23.59 23.59	23.29 23.57	0.95 s 0.52 s	-0.04 -0.05	-3.58 -4.11	$0.10 \\ 0.15$	$\begin{array}{c} 0.06\\ 0.05 \end{array}$	26.71 26.84
2-787.0 4-403.0	24.66 24.78	25.67 25.10	0.92 p 1.32 p	$0.13 \\ 0.17$	$3.09 \\ 5.79$	0.12 0.11	$\begin{array}{c} 0.06\\ 0.16\end{array}$	27.92 27.03
4-327.0 4-344.0	26.67 26.93	27.35 27.35	1.88 p 1.40 p	-0.36 -0.36	-3.33 -3.30	$\begin{array}{c} 0.07\\ 0.07\end{array}$	0.03 0.03	28.45 28.46

Table 1. Variable Galaxies in the HDF

Bandpass	$m_{AB}{}^{\mathrm{a}}$	δ epoch (days) ^b	δm^{c}
F300W	25.32	+732	-0.37 ± 0.05
F606W	20.52 22.52	-190	-0.02 ± 0.03
F814W	21.35	+732	-0.088 ± 0.012

Table 2. Photometric Changes of 2-251.0

 $^{\rm a}{\rm Isophotal}$ magnitudes in AB system from Williams et~al. 1996.

^bDifference between epochs in days relative to the primary HDF observations.

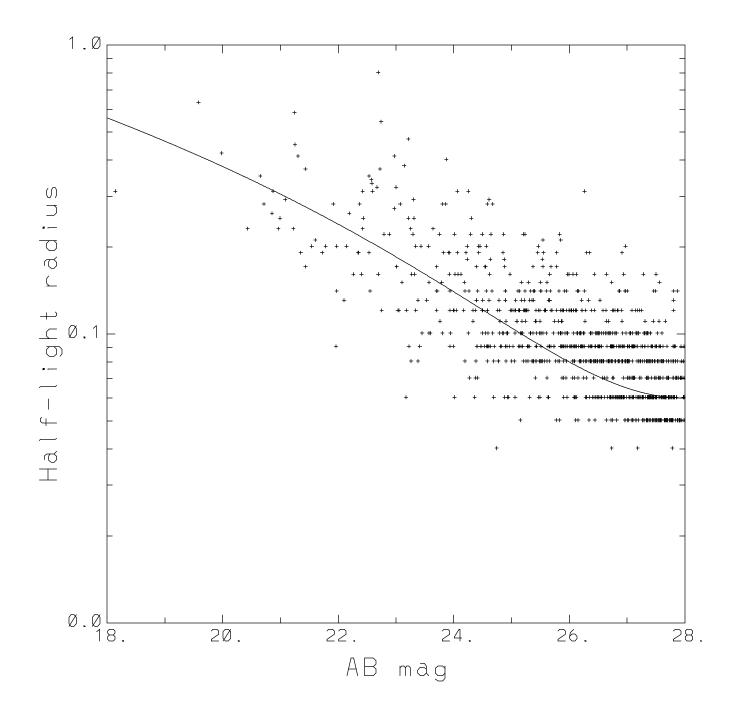
^cDifference in magnitudes always in the sense of later epoch relative to the earlier.

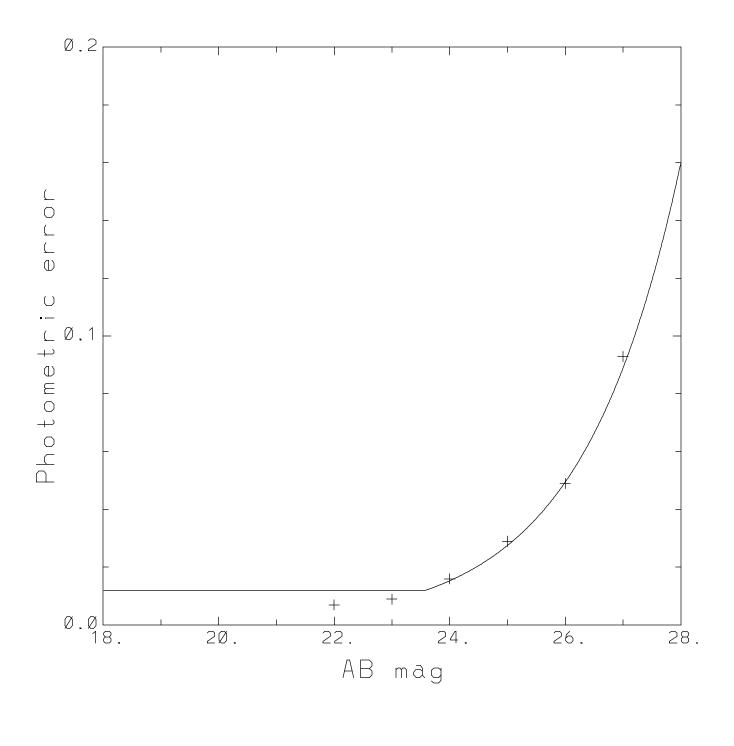
ID	m _{AB(8140)}	M_B	Z _{max}	V_a
4-260	22.55	-17.6648	2.11	4596.81
3-404	23.59	-14.8284	0.66	632.229
3-266	23.59	-16.1090	1.02	1479.11
2-787	24.66	-16.2056	1.46	2697.36
2-210	22.69	-16.7188	1.38	2453.97
2-251	21.24	-19.3116	4.41	10516.23

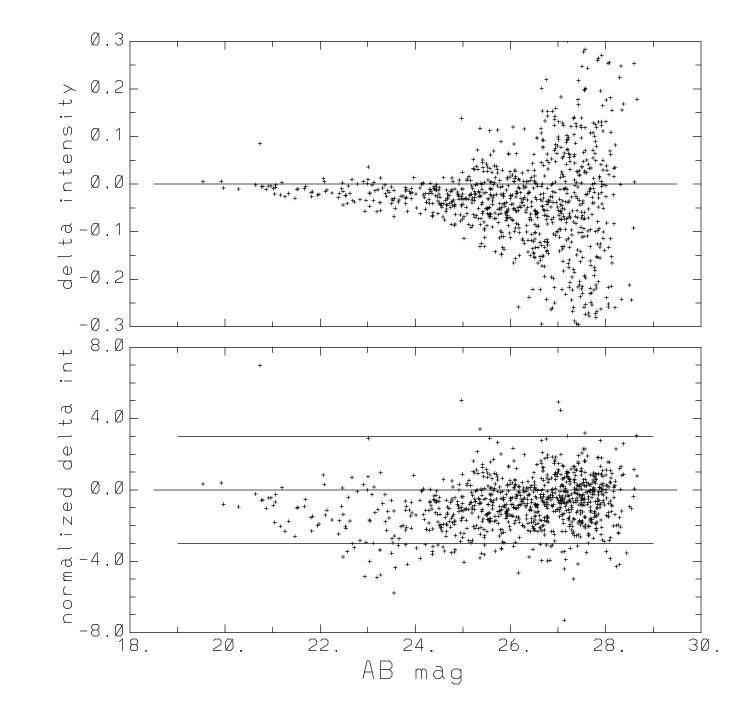
Table 3. AGN Component of HDF Variable Galaxies

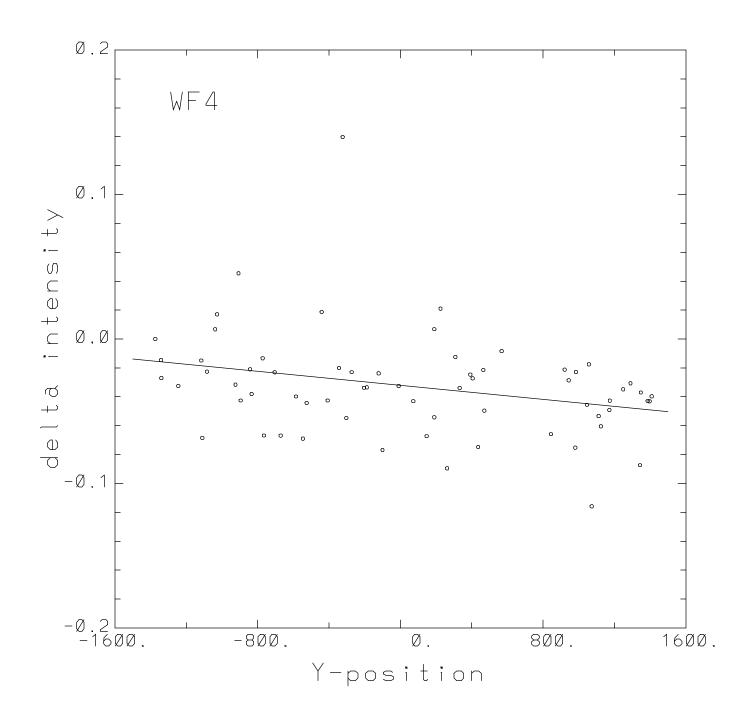
 Table 4.
 Luminosity Function for HDF Variable Galaxies

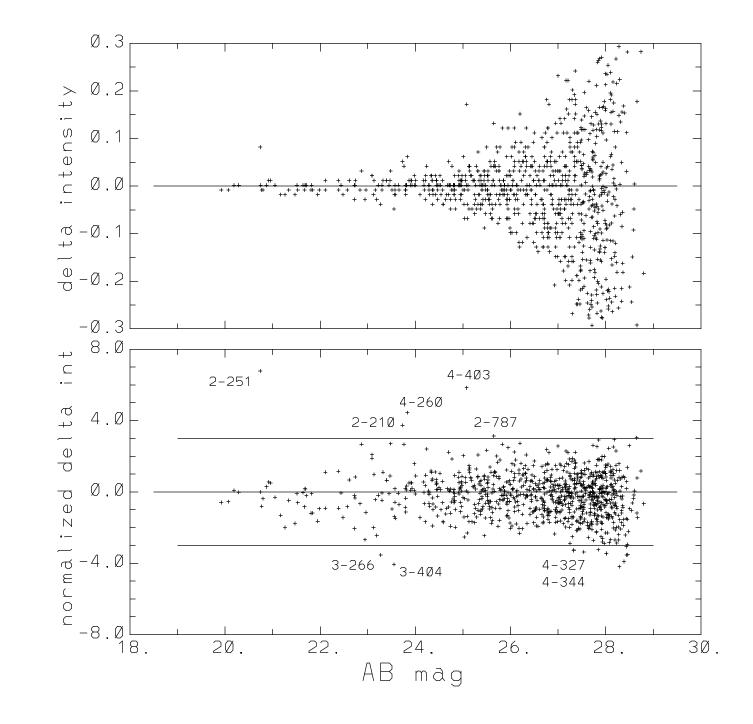
M_B	ϕ	n
-15.75	-3.51	4
-18.25	-4.13	2











 \log_{e} (Cumulative #)

